JBC RESEARCH ARTICLE

The small molecule DIPQUO promotes osteogenic differentiation *via* inhibition of glycogen synthase kinase 3-beta signaling

Received for publication, February 20, 2021, and in revised form, April 12, 2021 Published, Papers in Press, April 22, 2021,
https://doi.org/10.1016/j.jbc.2021.100696

Brandoch Cook[1,*], **Nicholas Walker**[1,2], **Qisheng Zhang**[3], **Shuibing Chen**[1], **and Todd Evans**[1]

From the [1]*Department of Surgery and* [2]*Program in Physiology, Biophysics & Systems Biology, Weill Cornell Medicine, New York, New York, USA; and* [3]*Department of Pharmacology, University of North Carolina, Chapel Hill, North Carolina, USA*

Edited by Roger Colbran

Bone fractures are common impact injuries typically resolved through natural processes of osteogenic regeneration and bone remodeling, restoring the biological and mechanical function. However, dysfunctionality in bone healing and repair often arises in the context of aging-related chronic disorders, such as Alzheimer's disease (AD). There is unmet need for effective pharmacological modulators of osteogenic differentiation and an opportunity to probe the complex links between bone biology and cognitive disorders. We previously discovered the small molecule DIPQUO, which promotes osteoblast differentiation and bone mineralization in mouse and human cell culture models, and in zebrafish developmental and regenerative models. Here, we examined the detailed function of this molecule. First, we used kinase profiling, cellular thermal shift assays, and functional studies to identify glycogen synthase kinase 3-beta (GSK3-β) inhibition as a mechanism of DIPQUO action. Treatment of mouse C2C12 myoblasts with DIPQUO promoted alkaline phosphatase expression and activity, which could be enhanced synergistically by treatment with other GSK3-β inhibitors. Suppression of the expression or function of GSK3-β attenuated DIPQUO-dependent osteogenic differentiation. In addition, DIPQUO synergized with GSK3-β inhibitors to stimulate expression of osteoblast genes in human multipotent progenitors. Accordingly, DIPQUO promoted accumulation and activation of β-catenin. Moreover, DIPQUO suppressed activation of tau microtubule-associated protein, an AD-related effector of GSK3-β signaling. Therefore, DIPQUO has potential as both a lead candidate for bone therapeutic development and a pharmacological modulator of GSK3-β signaling in cell culture and animal models of disorders including AD.

Although bone fracture is among the most common tissue injuries requiring emergent care, human bone can recover integrity through scarless regeneration. Unfortunately, osteoporosis and impaired fracture healing are part of a panoply of aging-related maladies that impede the seamless regeneration of new bone with structural and biomechanical integrity. These in turn are prominent comorbidities associated with chronic disorders such as Alzheimer's disease (AD) (1–4), resulting in poor prognoses and reduced quality of life for affected patients. There is therefore an unmet need for scalable and effective therapies that stimulate osteogenic recovery, regeneration, and differentiation. We recently discovered the osteogenic small molecule DIPQUO in a high-throughput chemical screen for novel activators of alkaline phosphatase (ALP), a marker for differentiation from mesenchyme progenitors toward the bone (5). DIPQUO additionally promotes matrix mineralization of differentiating human mesenchymal cells, ossification of larval zebrafish vertebrae, and osteoblastogenic regenerative processes in recovering adult zebrafish blastema. These properties together mark DIPQUO as a strong lead candidate bone anabolic compound.

Our previous study identified activation of p38 mitogen-activated protein kinase (MAPK)-β as a prime mechanistic driver of DIPQUO-mediated biological activity (5). However, p38 MAPK signaling operates either in parallel or downstream of a wide array of other developmentally important kinase and cytokine activities that impact essential developmental patterning as well as osteogenic differentiation and development (6), including transforming growth factor-beta (7), bone morphogenetic protein (BMP) (8, 9), extracellular signal–regulated kinase (ERK) (10, 11), fibroblast growth factors (12–14), and phosphoinositide 3-kinase/protein kinase B signaling (15, 16). In addition, canonical Wnt signaling through glycogen synthase kinase 3-beta (GSK3-β) plays important developmental and maintenance roles in osteogenic differentiation in both embryonic and adult tissues (17).

In our previous study, the timing of p38 MAPK activation peaked between 2 and 4 h after DIPQUO treatment of myoblast cells, subsequently declining quickly back to baseline levels. This observation, combined with persistent changes in cell morphology and sustained activation of osteogenic programs, suggests additional relevant direct and/or indirect effector pathways impacted by DIPQUO treatment. In addition, structure–activity relationship studies indicated that observed osteogenic differentiation was dependent upon its unique structure and that modification of structural moieties attenuated its activity,

* For correspondence: Brandoch Cook, brc2018@med.cornell.edu.

precluding an affinity-based approach to target identification. Therefore, we hypothesized that DIPQUO would impact a biochemical effector pathway upstream of p38 with therapeutic relevance in the bone, thus substantiating continued development of DIPQUO as a lead candidate bone therapeutic, and as a platform to combine the study of bone disorders and aging-related comorbidities. In the present study, we sought to identify kinases modulated by DIPQUO in a strategy to find molecular therapeutic effectors to pursue in future lead optimization studies. Through kinase profiling, biochemical and functional studies, we have identified GSK3-β signaling as an effector of DIPQUO pro-osteogenic activity.

Results

Kinase profiling and cellular thermal shift assays identify GSK3-β as a biochemical and functional effector of DIPQUO

To identify direct or indirect biochemical effectors of DIPQUO, we initiated a series of *in vitro* kinase assays, in which a panel of 60 kinases was selected based on published evidence of activity in osteogenesis and adipogenesis and tested for activation or inhibition by 10 μM DIPQUO. These tests were performed in duplicate, and only GSK3-β displayed 100% inhibition in both replicate assays (Fig. 1*A*). For clarity, only kinases that displayed positive values (inhibition) are displayed in Figure 1*A*, with a 70% inhibition threshold marked (dotted red line) above which they were tested for further validation with specific inhibitors. In addition to GSK3-β, the following kinases were found to be inhibited >70% by DIPQUO: AMP-activated protein kinase, cyclin-dependent kinase (CDK) 1 and CDK5, checkpoint kinase-1 and checkpoint kinase-2 (CHK1/2), serine/threonine kinase D2, serine/threonine protein kinase-4, -3, and -24/mammalian sterile twenty-like-1 -2 and 3 (MST1/2/3), and leucine-rich repeat kinase-2 (LRRK2; Fig. 1*A*).

Subsequent experiments validated GSK3-β as a biochemical effector of DIPQUO. First, the cellular thermal shift assay (CETSA) (18, 19) was used to measure the conformational stability imparted to GSK3-β by DIPQUO compared with an inactive chemical analog (BT344) (5), with cell extracts subjected to increasing temperatures (Fig. 1*B*). In principle, the binding of a compound to its cognate protein target increases the enthalpy required for its unfolding and denaturation, observable as an upward shift in the melting temperature (T_m), measured as the temperature at which 50 percent of measured protein remains in the solution. In practice, application of a CETSA temperature gradient results in additional stabilization of target-dependent protein–protein interactions and multiprotein complexes, such that an observed stabilization can identify a given protein as either a direct target or as a member of a functional protein complex. The dynamics of protein stabilization are dependent on the kinetics of compound–target engagement and are thus transitory, with stabilization preceding inhibition, depletion, or activation of targets and dissolution of relevant complexes. Through the CETSA, the associated chronology can be empirically determined. As shown in Figure 1*B*, the T_m for GSK3-β in DIPQUO-treated samples was measured to be 54.9 °C, compared with a T_m of 53.1 °C for analog-treated samples, with a statistically significant difference between respective protein levels bracketing those temperatures. Stabilization of GSK3-β occurred after 1 h of DIPQUO treatment, whereas in our published studies, p38 MAPK activation was maximal at later time points, between 2 and 4 h of treatment.

Previous studies identified a role for GSK3-β in the control of ALP expression and activity (20), with the common Wnt signaling activator CHIR99021 (CHIR) known to promote ALP activity in embryonic stem cells (21), and this activity for CHIR was confirmed in C2C12 myoblasts (Fig. 1*C*). In a similar manner to CHIR, C2C12 cells were treated with the direct AstraZeneca GSK3-β-specific inhibitor AZD2858 (AZD) (22) and found to stimulate expression of ALP (bright purple foci; Fig. 1*C*). Although the reported *in vitro* IC_{50} for CHIR and AZD are 6.7 and 68 nM, respectively, treatments were titrated (not shown) to determine the dose at which positive staining would consistently be observed (10 μM for CHIR and 1 μM for AZD). Analogously, the time point of 3 days was determined to be optimal to resolve ALP staining and activity for samples treated with DIPQUO and commercial GSK3-β inhibitors (also not shown). Colorimetric ALP activity assays showed that both CHIR and AZD promoted significant ALP activity to levels comparable with DIPQUO-induced stimulation (Fig. 1*D*).

Among the kinases identified in the profiling screen as > 70% inhibited, only GSK3-β was confirmed *via* functional assays using ALP expression as a readout. In these staining assays, expression of ALP is denoted by bright purple hematoxylin-positive foci (Fig. S1). Equivalent high-dosage treatment of C2C12 cells with commercially available inhibitors to all other candidate kinases failed to yield detectable ALP staining (Fig. 2*A*). Qualitative presence of ALP-positive hematoxylin-stained foci correlates to quantitative increase in ALP activity *via* colorimetric measurement of substrate digestion, as shown in Figs. 1C and 3, *A*–*C* (see below), whereas the absence of stained foci signifies lack of activity. Therefore, in experiments for which there was no ALP-positive staining in any sample, those negative samples were not subjected to quantification of activity (all of Fig. 2). For analysis of other kinase pathways, cells were treated with dorsomorphin (AMP-activated protein kinase and activin receptor-like kinase-2/3/6 inhibitor, 5 μM); PV1019 (Chk1/2 inhibitor, 10 μM); CHK2inhII (Chk2 inhibitor, 10 μM); RO-3306 (CDK1 inhibitor, 10 μM); roscovitine (CDK1/2/5 inhibitor, 10 μM); CRT006 (PKD1/2/3 inhibitor, 5 μM); XMU-MP-1 (mammalian sterile twenty-like 1/2 inhibitor, 5 μM); bosutinib (BCR-ABL and mammalian sterile twenty-like 3 inhibitor, 5 μM); and LRRK2-IN-1 or GSK2578215A (LRRK2 inhibitors, 10 μM). For all kinase inhibitors, treatments were titrated to empirically determine the highest dose resulting in the least cell depletion. In all cases, neither lowest- nor highest-dose treatment resulted in positive ALP staining (not shown). In addition, cotreatment

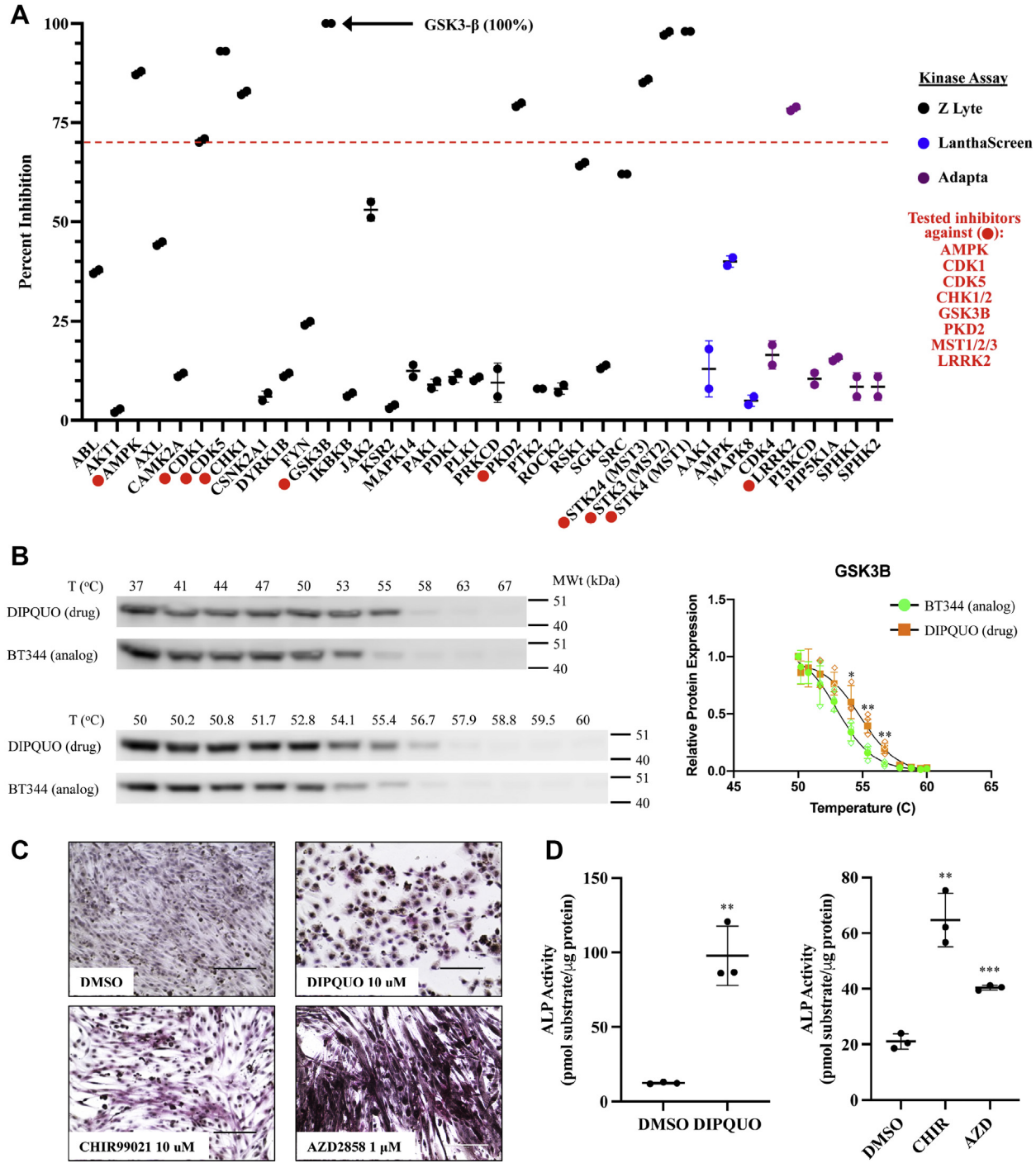

Figure 1. Kinase profiling identifies GSK3-β as a biochemical effector of DIPQUO-mediated inhibition. *A*, to identify putative biochemical effector candidates for DIPQUO, *in vitro* FRET-based kinase profiling assays were performed using 10 μM DIPQUO. Sixty different kinases were tested in duplicate using Z′-LYTE (*black spheres*), LanthaScreen (*blue spheres*), and Adapta (*purple spheres*) assays. Kinases were scored for inhibition (positive scores) or activation (negative scores); for clarity and brevity, only positive scores are shown, with an arbitrary threshold of 70% inhibition (*red dotted line*) chosen for follow-up validation assays, with kinases achieving this threshold denoted by *red spheres* on graph *x*-axis, and in *red print* on the sidebar. Only GSK3-β (*black arrow*) displayed 100% inhibition, in both duplicate tests. Values are reported as the means ± SD. *B*, cellular thermal shift assay (CETSA) analysis of GSK3-β protein stability after 1 h of 10 μM DIPQUO treatment in C2C12 cells, compared with treatment with the inactive structural analog BT344 (also 10 μM). CETSA was performed across a broad temperature range (37–67 °C, *upper panel*) and a narrow range (50–60 °C, *lower panel*). Relative protein levels were quantified at each temperature gradient point from 50 to 60 °C in a 10-min thermal challenge and plotted on the graph at right in a decay curve to obtain a T_m (50 percent relative expression) of 53.1 °C for BT344 and 54.9 °C for DIPQUO. Values are reported as the means ± SD; $*p < 0.05$ and $**p < 0.01$ in unpaired two-tailed Student's *t* test. Two-way ANOVA yielded F = 3.805 and $p = 0.0096$. Inhibition of GSK3-β using indicated doses of the commercially available inhibitors CHIR99021 (CHIR) or AZD2858 (AZD) stimulated (*C*) ALP expression and (*D*) ALP enzymatic activity. Expression was detected using alkaline naphthol and hematoxylin staining, and activity was quantified using colorimetric analysis of pNPP substrate digestion, after 3-day treatment of C2C12 cells with 10 μM DIPQUO. Activity was normalized to the total protein content for each sample. Values are reported as the means ± S.D.; $**p < 0.01$ and $***p < 0.001$ in unpaired two-tailed Student's *t* test. Ordinary one-way ANOVA yielded F = 42.95 and $p = 0.0003$. The scale bar in *panel C* represents 200 μm. In all panels, representative images are shown for experiments performed in three biological replicates. ALP, alkaline phosphatase; GSK3-β, glycogen synthase kinase 3-beta; pNPP, p-nitrophenylphosphate; T_m, melting temperature.

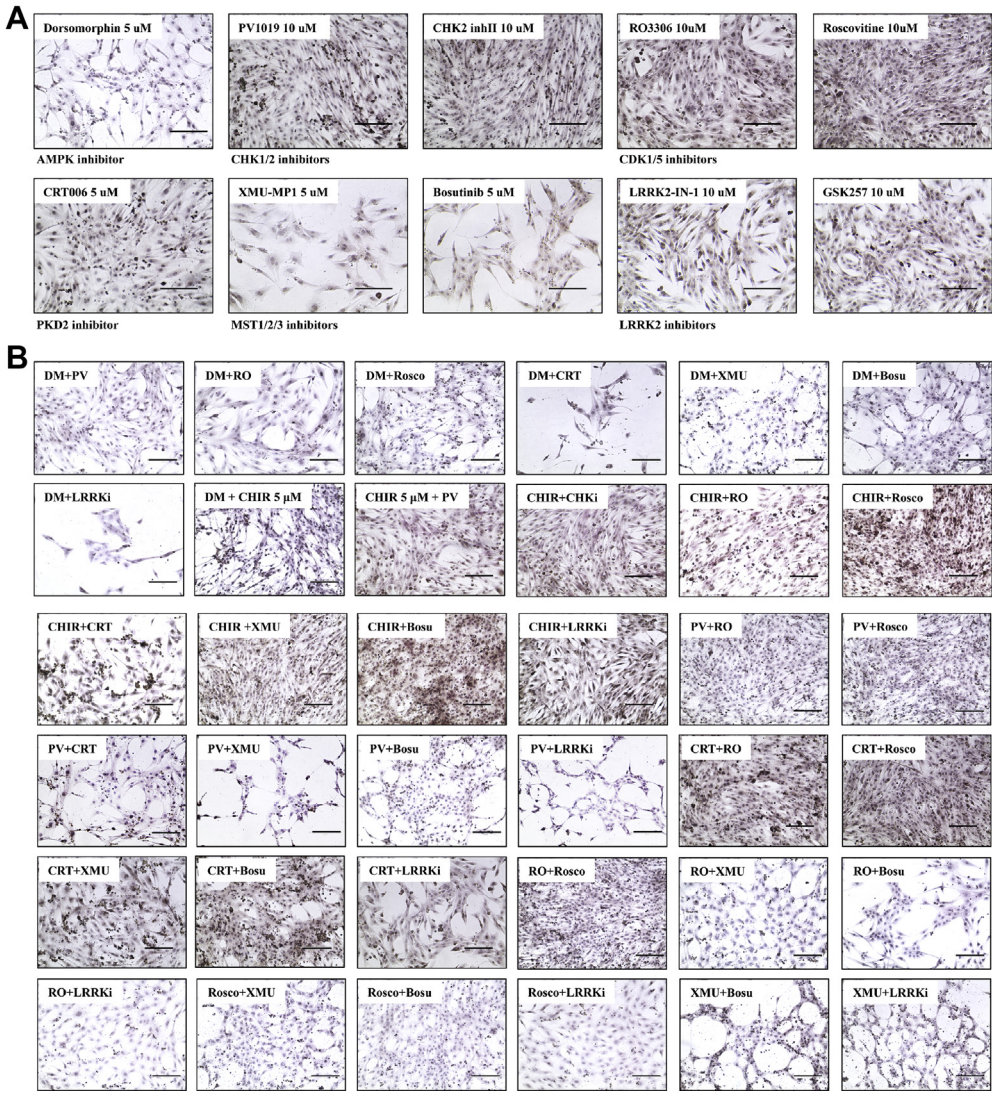

Figure 2. Small-molecule inhibition of other putative kinase effectors fails to promote alkaline phosphatase expression. *A*, for all other kinases that displayed >70% inhibition by DIPQUO in the profiling assay, C2C12 cells were treated for 3 days with commercially available small-molecule inhibitors in the concentrations shown and stained for ALP expression. Inhibitors were as follows: dorsomorphin (DM), PV1019 (PV), Chk2inhII (Chki), RO3306 (RO), roscovitine (Rosco), CRT006 (CRT), XMU-MP-1 (XMU), Bosutinib (Bosu), LRRK2-IN-1 (LRRKi), and GSK2578215a (GSK257). The scale bar represents 200 µm. *B*, cells were similarly treated with dual combinations of the same kinase inhibitors (for each kinase, only one inhibitor was chosen based on availability) to assess whether simultaneous inhibition of different pathways would synergize to result in ALP expression. Treatments were performed at the same concentrations, with the exception of CHIR treatment, which was used at a concentration determined empirically to be subthreshold for ALP staining. For all panels, representative images are shown from experiments that were performed in at least three biological replicates. The scale bar represents 200 µm. ALP, alkaline phosphatase; CHIR, Wnt signaling activator CHIR99021.

with all possible combinations to simultaneously inhibit two kinases ruled out synergistic effects between any of these biochemical pathways to promote detectable ALP expression (Fig. 2*B*).

DIPQUO can synergize with other known GSK3-β inhibitors to stimulate osteoblast-like differentiation

DIPQUO and other GSK3-β inhibitors were next tested for their ability to synergize in functional, biochemical, and molecular assays to measure osteogenic potential. When subthreshold concentrations of the small-molecule GSK3-β inhibitors CHIR (5 µM) or AZD (500 nM) were used to treat C2C12 cells for 3 days, cell staining and activity assays failed to yield detectable ALP staining or enzymatic activity using the added p-nitrophenylphosphate (pNPP) substrate (Fig. 3, *A* and *B*). These concentrations were determined empirically for the purposes of this study (data not shown) and are well above published EC_{50} values for both inhibitors, suggesting that stimulation of ALP by either molecule is secondary to its primary target. Similarly, treatment of C2C12 cells with 5 µM DIPQUO failed to yield ALP staining or significant activity (Fig. 3, *A* and *B*). However, combination of subthreshold doses of DIPQUO with CHIR (Fig. 3*A*) or DIPQUO with AZD (Fig. 3*B*) resulted in robust ALP staining and significantly increased (>10-fold) ALP activity. Because combining the subthreshold levels of individual compounds recapitulates activity found using super-threshold levels of either

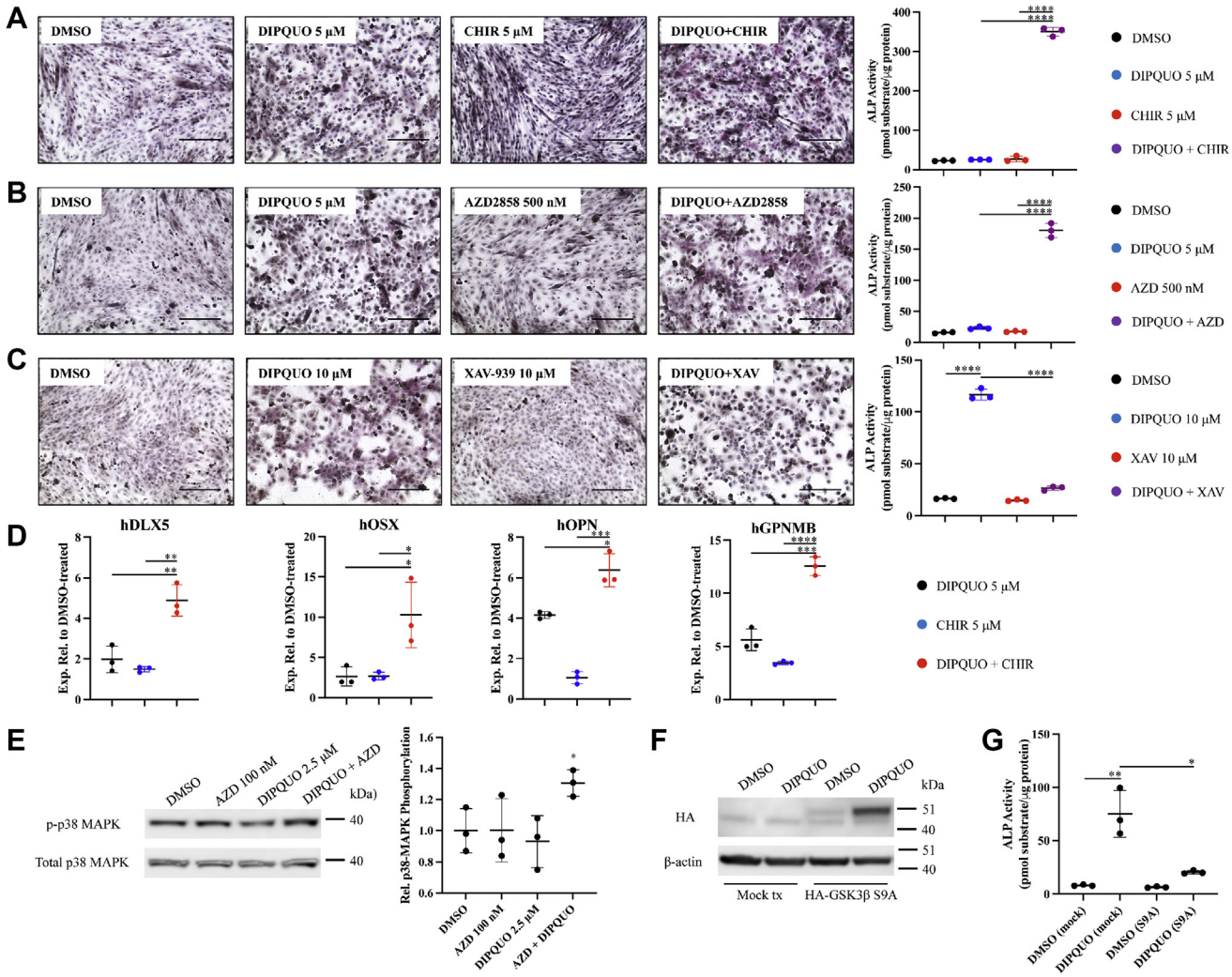

Figure 3. DIPQUO can synergize with other known GSK3-β inhibitors to promote osteogenic differentiation. C2C12 cells were treated for 3 days with (*A*) subthreshold (5 μM) DIPQUO, (5 μM) CHIR, or a combination thereof or (*B*) subthreshold DIPQUO, (500 nM) AZD, or a combination thereof and analyzed by staining for ALP expression and by colorimetric substrate assay for ALP activity. *C*, ALP expression and activation normally promoted by the full dose of DIPQUO was attenuated by cotreating C2C12 cells with 10 μM XAV-939. The scale bar in *panels A–C* represents 200 μm. Values in ALP activity graphs are reported as the means ± SD; ****$p < 0.0001$ in unpaired two-tailed Student's *t* test. Ordinary one-way ANOVA yielded F = 1868 and $p < 0.0001$ in *panel A*, F = 579.6 and $p < 0.0001$ in *panel B*, and F = 858.3 and $p < 0.0001$ in *panel C*. *D*, differentiating human skeletal muscle satellite cells were cotreated for 3 days with low-dose DIPQUO and CHIR (5 μM each) and then analyzed by quantitative RT-PCR for expression of transcripts associated with osteoblast specification, compared with treatment alone. Relative expression levels compared with DMSO-treated samples and normalized to glyceraldehyde 3-phosphate dehydrogenase are reported as the means ± SD; *$p < 0.05$, **$p < 0.01$, ***$p < 0.001$, and ****$p < 0.0001$ in unpaired two-tailed Student's *t* test. Ordinary one-way ANOVA yielded F = 29.08 and $p = 0.0008$ for hDLX5 (*DISTAL-LESS HOMEOBOX* 5); F = 9.654 and $p = 0.0133$ for hOSX (*OSTERIX*); F = 81.15 and $p < 0.0001$ for hOPN (*OSTEOPONTIN*); and F = 110.1 and $p < 0.0001$ for hGPNMB (*OSTEOACTIVIN*). *E*, synergistic activation of p38 MAPK was analyzed by Western blotting after 2.5 h treatment with subthreshold concentrations of AZD (100 nM) and DIPQUO (2.5 μM), compared with cotreatment using the same concentrations. Relative phospho-p38 MAPK levels are reported as the means ± SD; *$p < 0.05$. Ordinary one-way ANOVA yielded F = 3.521 and $p = 0.0686$. *F*, C2C12 cells were either mock-transfected or transfected for 24 h with hemagglutinin-tagged GSK3-β containing a serine-to-alanine mutation (S9A), treated with DIPQUO or DMSO vehicle, and analyzed by Western blotting for construct expression. *G*, equivalent samples were analyzed for ALP activity using colorimetric assay for pNPP substrate after 3 days. Activity levels are normalized to the total protein and reported as the mean ± SD; *$p < 0.05$ and **$p < 0.01$ in unpaired two-tailed Student's *t* test. Ordinary one-way ANOVA yielded F = 25.60 and $p = 0.0002$. In all figure panels, representative images are shown from at least three biological replicates. ALP, alkaline phosphatase; AZD, AstraZeneca GSK3-β-specific inhibitor AZD2858; CHIR, Wnt signaling activator CHIR99021; GSK3-β, glycogen synthase kinase 3-beta; pNPP, p-nitrophenylphosphate.

compound, this is good evidence that they act on the same pathway. Accordingly, attenuation of Wnt signaling with the small-molecule tankyrase inhibitor XAV-939, which effectively acts to protect GSK3-β activity, blocked the promotion of ALP expression and activity with the full effective 10 μM dose of DIPQUO (Fig. 3*C*).

Analogous to murine C2C12 cells, human skeletal muscle satellite cells (hSkMSCs) are mesenchymal progenitors that retain potential to differentiate toward myogenic, adipogenic, or osteogenic lineages in a manner dependent on culture conditions (23, 24). Therefore, they serve as a supporting model to re-evaluate and confirm the ability of DIPQUO to synergize with GSK3-β inhibition in human and murine cells, promoting osteogenic differentiation. In hSkMSC cultures, cotreatment for 3 days with subthreshold doses of DIPQUO and CHIR resulted in significantly

increased expression of osteoblast marker genes, including *DLX5*, *OSTERIX*, *OSTEOPONTIN*, and *GPNMB* (*OSTEOACTIVIN*; Fig. 3*D*). To measure synergistic effects of DIPQUO with established GSK3-β inhibitors on a biochemical pathway indicative of osteogenic differentiation, C2C12 cells were cotreated with subthreshold doses of DIPQUO and AZD and then probed for activation of p38 MAPK, which we previously showed is required for DIPQUO-induced differentiation, and is a known conserved pathway in skeletal differentiation and patterning (5, 7). Western blotting analysis showed that phosphorylation of p38 MAPK is significantly increased only in response to the combinatorial application of low-dose DIPQUO and AZD (Fig. 3*E*). Therefore, several biological readouts, encompassing (1) expression and activity of the osteogenic enzyme ALP in murine cells; (2) transcriptional activation of osteoblast markers in human progenitors; and (3) activation of MAPK signaling through p38 indicate that combinatorial GSK3-β inhibition using DIPQUO and other commercially available inhibitors stimulates osteogenic programs in both mouse and human cell culture models.

Accordingly, osteogenic outcomes are dependent on proper biological function of GSK3-β signaling. When C2C12 cells were transfected with a constitutively active GSK3-β construct containing a serine-to-alanine mutation (S9A; Fig. 3*F*) to compete with endogenous GSK3-β, DIPQUO induction of ALP activation was significantly suppressed (Fig. 3*G*).

DIPQUO promotes β-catenin accumulation and activity

Signaling through the canonical Wnt pathway leads to deactivation and sequestration of normally constitutively active GSK3-β away from interacting partners including axin and adenomatous polyposis coli (25). As a result, β-catenin is dephosphorylated and accumulates in the nucleus, where it triggers transcriptional activation of target genes that can promote cell proliferation and differentiation in many developmental contexts, including osteogenesis (26). To further validate DIPQUO as an inhibitor of GSK3-β biochemical activity, we investigated β-catenin expression and activation of transcriptional targets. In Western blotting analyses of DIPQUO-treated C2C12 cells, total β-catenin accumulated over time, increasing approximately 3-fold by 24 h of treatment compared with dimethyl sulfoxide (DMSO)-treated samples (Fig. 4*A*). Accumulation of β-catenin was additionally dose dependent, with a maximum observed at the 10-μM concentration used throughout this study as a baseline for promoting osteogenic differentiation (Fig. 4*B*). Although there was a consistent upward dose-dependent trend, significant accumulation first occurred at the 7.5 μM dose, in a similar range as the original calculated EC_{50} of 6.28 μM. To measure β-catenin activity, a lentivirus containing a T-cell factor/lymphoid enhancer-binding factor transcriptional response element-conjugated GFP luciferase reporter was used to infect 293T cells (Fig. 4*C*). Cells treated for 24 h with 10 μM DIPQUO or CHIR were normalized to

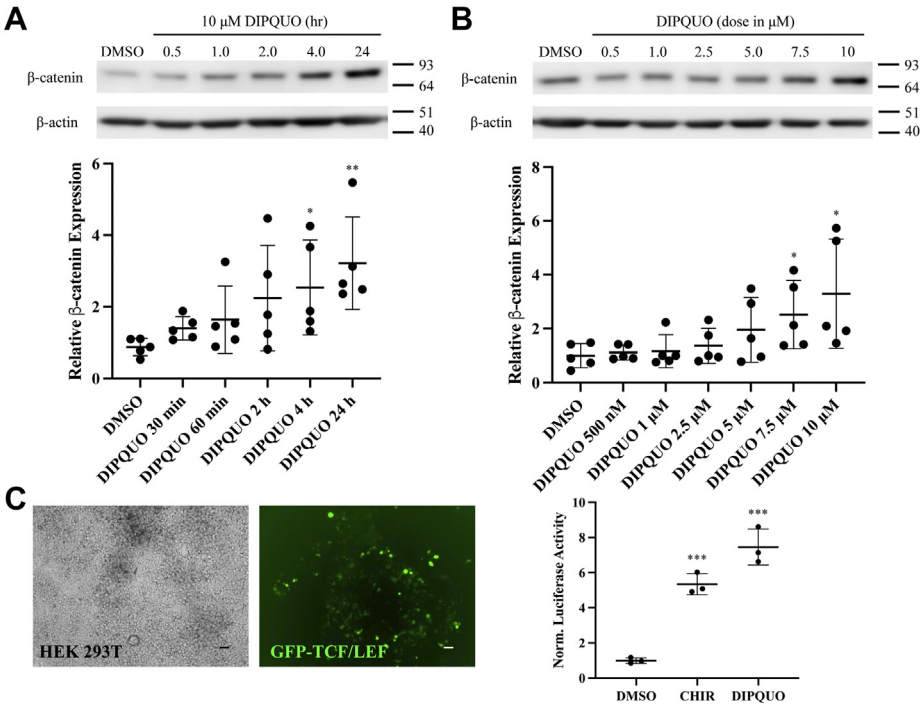

Figure 4. DIPQUO promotes β-catenin accumulation and activity. C2C12 cells were treated with DIPQUO for (*A*) time periods and (*B*) doses indicated in time-course and dose–response analyses to examine β-catenin expression levels by Western blotting in whole-cell extracts. Associated graphs below show expression levels compared with DMSO-treated controls. Relative β-catenin levels are reported as the means ± SD; *$p < 0.05$ and **$p < 0.01$ in unpaired two-tailed Student's *t* test. Ordinary one-way ANOVA yielded F = 3.237 and $p = 0.0225$ in *panel A* and F =3.170 and $p = 0.0168$ in *panel B*. *C*, luciferase activity assay using transient expression of GFP-T-cell factor/lymphoid enhancer-binding factor lentivirus (MOI = 20) in 293T cells, followed by treatment with DMSO, 10 μM CHIR or 10 μM DIPQUO. The scale bar represents 50 μm. Luciferase activity normalized to DMSO-treated samples is reported as the mean ± SD; ***$p < 0.001$ in unpaired two-tailed Student's *t* test. Ordinary one-way ANOVA yielded F = 67.84 and $p < 0.0001$. Representative images from experiments using at least three biological replicates are shown for all figure panels. MOI, multiplicity of infection; CHIR, Wnt signaling activator CHIR99021.

DMSO-treated controls for luminescence and were found to display significantly increased luciferase activity. DIPQUO treatment additionally showed an upward trend compared with CHIR-positive controls, with activity approximately 7.5-fold greater than DMSO-negative controls (Fig. 4*C*).

DIPQUO suppresses tau microtubule-associated protein phosphorylation

Several published reports have identified GSK3-β as a regulator of tau microtubule-associated protein activation, which is commonly observed in neurofibrillary tangles associated with AD etiology (27–29). Tau has been widely studied as a candidate AD therapeutic target, including attempts to generate safe and effective anti-GSK3-β treatments that control tau phosphorylation and impact neurodegenerative tauopathy (30). Therefore, we hypothesized that DIPQUO treatment in cell culture would impact tau phosphorylation, in its capacity as a GSK3-β substrate. To substantiate biochemical function of DIPQUO through GSK3-β in this manner, we performed Western blotting analysis of phospho-tau. In NIH/3T3 cells overexpressing human 4-repeat WT tau (4R0N), treatment with 10 μM DIPQUO significantly reduced phosphorylation of serine-396 (S396), a modification of tau associated with overactivity and dysregulation of cytoskeletal architecture in AD (31) (Fig. 5*A*). Moreover, the dose–response analysis demonstrated that DIPQUO suppression of tau was approximately 10-fold more effective, with significant suppression observed at the 500 nM dose (Fig. 5*B*), compared with an EC_{50} originally measured at 6.28 μM for ALP activation (5). Tau is commonly phosphorylated on S396 by GSK3-β, and on as many as 40 other residues by several kinase signaling pathways, including CDK5 (32) and the MAPK family members ERK1/2 (33, 34), p38 MAPK-γ (35), and c-Jun terminal kinase (36, 37), all of which have been studied in AD and other contexts. In kinase profiling assays, no MAPK family members were identified as being inhibited or activated by DIPQUO (not shown). Although CDK5 was inhibited in duplicate kinase assays, subsequent testing using CDK5 inhibitors alone and in concert with subthreshold doses of CHIR09921 did not result in ALP expression (Fig. 2). Accordingly, phosphorylation of tau-T217 was moderately but not significantly suppressed by DIPQUO (Fig. 5*C*). This threonine is flanked by residues that comprise consensus sequence substrates for GSK3-β, CDK5, and MAPK family members (38). Therefore, inhibition of GSK3-β may not be sufficient to effect a strong suppression. However, inhibition of ERK1/2 signaling with UO126 in combination with DIPQUO did not impact tau phosphorylation on either S396 or T217, reinforcing the observation that DIPQUO specifically

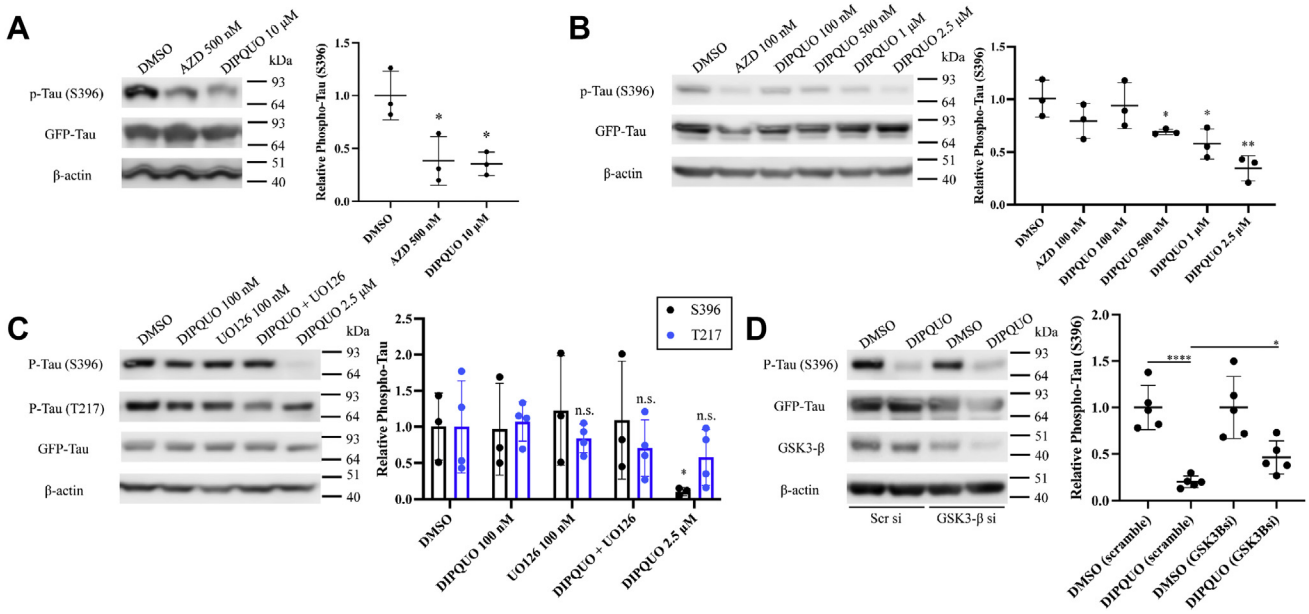

Figure 5. DIPQUO blocks phosphorylation of tau microtubule-associated protein. *A*, NIH/3T3 fibroblasts were transfected with GFP-tagged human four-repeat WT tau (4R0N) and treated with 500 nM AZD or 10 μM DIPQUO for 24 h and then analyzed by Western blotting for tau expression and activity *via* phosphorylation of S396. Phospho-S396-tau was quantified as a ratio to total tau in the graph at right. Values are reported as the means ± SD; $*p < 0.05$ in unpaired two-tailed Student's *t* test. Ordinary one-way ANOVA yielded F = 10.12 and $p = 0.0119$. *B*, further dose–response Western blotting analysis of tau S396 phosphorylation demonstrated a dose-dependent relationship for DIPQUO, with significant inhibition at the 500 nM dose. Values are reported as the means ± SD; $*p < 0.05$ and $**p < 0.01$ in unpaired two-tailed Student's *t* test. Ordinary one-way ANOVA yielded F = 7.549 and $p = 0.0020$. *C*, phosphorylation of tau S396 and T217 was analyzed after treatment with DIPQUO in the absence or presence of the ERK1/2 inhibitor UO126. Phospho-tau was quantified in the graph as a ratio to total tau, normalized to β-actin, with P-tau-S396 in *black* and P-tau-T217 in *blue*. Values are reported as the means ± SD; $*p < 0.05$ in unpaired two-tailed Student's *t* test. Two-way ANOVA yielded F = 1.235 and $p = 0.3296$. *D*, depletion of GSK3-β for 24 h with siRNA partially restored S396 phosphorylation of tau after an additional 24 h of 10 μM DIPQUO treatment. The graph at right shows ratio of phospho-S396-tau to total tau, normalized to β-actin protein loading control. Values are reported as the means ± SD; $*p < 0.05$ and $****p < 0.0001$ in unpaired two-tailed Student's *t* test. Ordinary one-way ANOVA yielded F = 15.61 and $p < 0.0001$. Representative images from experiments using at least three biological replicates are shown for all figure panels. AZD, AstraZeneca GSK3-β-specific inhibitor AZD2858; GSK3-β, glycogen synthase kinase 3-beta.

blocks GSK3-β biochemical activity (Fig. 5*C*). Finally, specific silencing of GSK3-β expression with siRNA partially blocked suppression of tau S396 phosphorylation, with an approximately 2.5-fold recovery of relative S396 phosphorylation in GSK3-β siRNA samples compared with scrambled siRNA controls (Fig. 5*D*).

Discussion

Through kinase profiling and functional assays, we identified GSK3-β as a biochemical effector of the candidate bone anabolic molecule DIPQUO. Although profiling revealed several kinases that were inhibited appreciably by DIPQUO, only GSK3-β was validated *via* induction of ALP expression and activity assays by treatment with kinase-specific, commercially available inhibitors and by the CETSA analysis of protein stability. Moreover, DIPQUO at subthreshold levels was able to synergize with other GSK3-β inhibitors to amplify ALP activity and promote downstream activation of p38 MAPK signaling in murine C2C12 myoblasts and stimulate expression of osteoblast genes in hSkMSCs. This is in interesting contrast to our previous study (5), which used recombinant BMP4 protein as a known osteogenic factor and as a screening and positive control. In that study, we found DIPQUO promoted higher expression of transcripts associated with osteoblast maturation than BMP4 and that it functioned in parallel to the BMP4 signaling pathway regarding both p38-MAPK activation and ALP expression. Our present results, however, show DIPQUO functioning in series with GSK3-β signaling. Consequently, DIPQUO additionally promoted accumulation of β-catenin and increased activity in a transcriptional reporter assay. Finally, inhibition of GSK3-β by DIPQUO suppressed phosphorylation of tau microtubule-associated protein, a known substrate of GSK3-β signaling, relevant to the etiology of AD, a disorder commonly closely associated with bone healing and remodeling defects. DIPQUO therefore has the potential to act as an investigative bridge between AD and bone disorders to further understand their related etiologies using *in vitro* and *in vivo* model systems and to serve as a strong lead candidate molecule to therapeutically target osteogenic dysfunction complicated by aging-related comorbidities.

Although DIPQUO functions as a GSK3-β inhibitor, it is unknown if GSK3-β is a direct molecular target. Rather, biochemical inhibition of GSK3-β signaling may be a precondition of DIPQUO-induced osteogenic differentiation. There is a wealth of literature identifying a dual role for GSK3-β signaling in osteogenesis and cognitive disorders, particularly AD. For instance, tissue-specific deletion in mice of GSK3-β in differentiating osteogenic lineages resulted in developmental delays in skeletogenesis and ossification (39). Approved and experimental inhibitors of GSK3-β in mood and cognitive disorders have additionally demonstrated impacts on osteogenic differentiation. Lithium chloride has been shown to stimulate osteoblast differentiation and increase bone mass and mineral density (40, 41), whereas AZD2858 increased trabecular and cortical bone mass and strength, accelerating selective intramembranous fracture healing in a rat model of bone biomechanics (22, 42). Therefore, modulation of GSK3-β resides in a nexus where bone biology and cognitive function intersect. Because DIPQUO is composed of quinolinone and imidazole moieties, it is structurally distinct from the AZD series of targeted inhibitors identified by AstraZeneca in screens of over two million compounds, where selective inhibition and druggability were highest with pyrazine and oxindole quinazoline structures (43). Therefore, it is unlikely that DIPQUO is a direct inhibitor. Approved and experimental direct GSK3-β inhibitors have been shown to mediate significant off-target effects, which in the case of the nonspecific inhibitor lithium chloride has made full understanding of its mechanism elusive and its application limited to symptomology in a range of mood disorders for which it is empirically effective (44). Several other specific inhibitors, notably AZD1080, which progressed through phase I clinical trials for AD, and AZD2858, which progressed through initial GLP toxicology studies, were subsequently removed from development pipelines. AZD2858 demonstrated genotoxicity in addition to targeting bile duct and other organs, and chronic gall bladder inflammation in phase I clinical trials for AZD1080 precluded its entry into phase II trials (43). The recent history of strategic pursuit of GSK3-β as a therapeutic target has therefore bolstered an approach based on cautious and measured pharmacological regulation, rather than direct or total inhibition.

A corollary of this complexity is in published observations of the wide array of mechanisms responsible for regulation of GSK3-β activity. GSK3-β is unusual among kinases in its ubiquity and its default active state, which can be suppressed by myriad means including both serine/threonine and tyrosine phosphorylation, sequestration within different protein complexes, changes in subcellular localization, and context-dependent and cell type–dependent selection of substrate specificity, from over 100 known substrates (45). The present study demonstrates that overexpression in C2C12 cells of constitutively active, serine phosphorylation-disabled GSK3-β blocks the osteogenic activity of DIPQUO (Fig. 3*G*). However, we propose that post-translational modification of GSK3-β is only one means by which DIPQUO regulates its activity and that this is an outcome dependent on initial binding and modulation of an upstream molecular target. In our analyses, we did not identify any affected pathways other than GSK3-β and did not identify our chosen osteogenic readouts in the context of inhibition of any other kinase pathway. Although we believe modulation of GSK3-β is an important outcome of DIPQUO treatment, we do not claim this is direct or the only impact. In summary, DIPQUO demonstrates high potential for therapeutic optimization as a bone anabolic molecule and as a biochemical inhibitor of GSK3-β signaling relevant to modeling of chronic disease states commonly associated with bone repair dysfunction.

Experimental procedures

Kinase profiling assays

A panel of 60 kinases identified for their potential roles in osteogenesis and adipogenesis was tested with three different kinase profiling assay platforms by the Thermo Fisher Scientific SelectScreen Biochemical Kinase Profiling Service. All

assays were based on reading of FRET. All kinase assays were conducted in duplicate, and values reported reflect only those that tested positive (inhibition) and not those with negative values (activation).

For Z'-LYTE assays, a two-step reaction transfers ATP γ-phosphate to ser/thr/tyr residues on a FRET peptide, and then, a site-specific protease cleaves unmodified peptides. The ratio calculated between coumarin FRET donor emission at 445 nm and fluorescein acceptor emission at 520 nm, after donor excitation at 400 nm, is the measure of kinase inhibition. DIPQUO was screened in this assay in 1% DMSO using bar-coded low-volume black 384-well plates (Corning 4514). The assay included a 100% inhibition control with no ATP, a 100% phosphorylation control with synthetically phosphorylated peptide, a 0% inhibition control consisting of active kinase to establish a minimum emission ratio, and an in-plate standard curve using known kinase inhibitors in ten-point titration. The kinase reaction proceeded for 60 min and the development reaction for 60 min before analysis on a fluorescent plate reader.

For LanthaScreen assays, binding of an Alexa Fluor 647–conjugated ATP-competitive tracer to a kinase is detected by the addition of a europium-labeled anti-tag antibody. Kinase binding is measured as the FRET signal, and displacement by an inhibitor is measured as loss of FRET signal. DIPQUO was screened in 1% DMSO using bar-coded low-volume white 384-well plates (Greiner 784207). The assay included a 0% displacement control without known inhibitor, and a 100% displacement control, with the highest concentration of the known inhibitor used determined empirically by ten-point titration. The binding assay reaction proceeded for 60 min before reading on a fluorescent plate reader and calculating the emission ratio of AF647 (665 nm) to europium (615 nm).

For Adapta assays, a kinase reaction is followed by ADP detection using an AF647-labeled tracer and a europium-labeled anti-ADP antibody, with EDTA to stop the kinase reaction. Displacement of the tracer by ADP from the kinase reaction decreases the FRET signal, and in the presence of an inhibitor, ADP formation is reduced, increasing the FRET signal. DIPQUO was screened in 1% DMSO using bar-coded low-volume white 384-well plates (Corning 4512). The assay included a 0% conversion (100% inhibition) control with addition of ATP to the detection step, but not the kinase reaction step, to determine the maximum emission ratio. Also included were a 100% conversion control using ADP instead of ATP, and a 0% inhibition control using active kinase to establish the minimum emission ratio. An in-plate standard curve using known kinase inhibitors in a 10-point titration was also established. The kinase reaction proceeded for 60 min, followed by 60 min of equilibration of detection reagents, and the emission ratio of AF647 (665 nm) to europium (615 nm) was calculated.

Cell culture experiments

C2C12 mouse myoblast (CRL-1772), NIH/3T3 mouse fibroblast (CRL-1658), and human embryonic kidney 293T (CRL-3216) cell lines were purchased from the American Type Culture Collection and cultured in Dulbecco's modified Eagle medium (DMEM) containing 10% fetal bovine serum. hSkMSCs were purchased from Lifeline Cell Technology (FC-0091) and cultured in complete StemLife Sk Medium (Lifeline LL-0069). To measure osteoblast differentiation, the culture medium was changed to DMEM containing 20% fetal bovine serum and 2.5 ng/ml basic fibroblast growth factor. Cells were treated with DMSO, 10 μM DIPQUO, or BT344 inactive analog (5), unless otherwise noted. C2C12 cells were treated with DIPQUO or other inhibitors for 3 days before staining, measuring ALP activity, or harvesting RNA. Inhibitors were obtained from the following sources: DIPQUO (ChemBridge 16707928), CHIR99021 (Stemcell Technologies 72054), AZD2858 (Selleck S7253), Dorsomorphin (Tocris 3093), PV1019 (Millipore 220488), Chk2 inhibitor II (Millipore 200486), RO3306 (Selleck S7747), R-roscovitine (Cayman 10009569), CRT0066101 (Cayman 15337), XMU-MP1 (Cayman 22083), bosutinib (Cayman 12030), LRRK2-IN-1 (Cayman 18094), GSK2578215A (Tocris 4629), and XAV-939 (Sigma X3004). An expression construct containing 4-repeat human WT 4R0N tau (pRK5-EGFP-tau, Addgene 46904) was transfected into 70% confluent NIH/3T3 cells using Lipofectamine LTX Plus reagent (Invitrogen 15338-100), and DIPQUO or inhibitor treatments were performed simultaneously. Protein expression was assayed by Western blotting after 24 h. A hemagglutinin-tagged GSK3-β construct containing an amino acid substitution of serine to alanine (HA-GSK3beta-S9A-pcDNA3, Addgene 14754) was similarly transfected and assayed in C2C12 cells, with assessment of ALP activity being done after 3 days.

For β-catenin transcriptional activity assays, 50% confluent 293T cells were infected with lentivirus expressing a T-cell factor/lymphoid enhancer-binding factor-dscGFP construct (System Biosciences pGreenfire1 pre-packaged virus) with multiplicity of infection = 20. After 48 h, virus-containing media were replaced with normal culture media and cells were treated with 10 μM DIPQUO or CHIR99021 for another 24 h. Cell lysates were harvested and processed using Promega Luciferase Assay System (E1500) and luminescence values read using a Turner TD-20e Luminometer.

For siRNA experiments, siRNA corresponding to exon 2 of mouse GSK3-β (Thermo Fisher Silencer Select, s80826) was transfected into C2C12 cells for 24 h using Lipofectamine RNAiMAX reagent (Thermo Fisher 13778075). Cells were simultaneously treated for 24 h with DMSO or 10 μM DIPQUO. The expression level of GSK3-β was compared by Western blotting with cells transfected with a negative control siRNA (Ambion Silencer, Thermo Fisher AM4611).

Western blotting

Whole-cell extracts were collected from C2C12 or NIH/3T3 cells in the complete lysis buffer (20 mM Tris, 150 mM NaCl, 50 mM NaF, 1% NP-40 substitute, Halt protease, and phosphatase inhibitor cocktail from Thermo Scientific). Proteins were resolved by electrophoresis on precast 10% or 4 to 12% NuPAGE Bis-Tris gels (Invitrogen) and transferred to polyvinylidene fluoride membranes (Bio-Rad). Membranes were blocked in 5% bovine serum albumin in Tris buffered saline +

0.5% Tween-20 and then incubated at 4 °C overnight with primary antibodies. Antibodies used were as follows: rabbit anti-GSK3 (cat. No. 5676), anti-β-catenin (9562), anti-phospho-T180/Y182-p38 MAPK (9211), anti-p38 MAPK-XP (8690), anti-tau-XP (46687), anti-hemagglutinin (3724), mouse anti-phospho-S396-tau (9632; all from Cell Signaling Technology); rabbit anti-phospho-T217-tau (Abcam 192665); and mouse anti-β-actin (Sigma A1978). Proteins were visualized using horseradish peroxidase-conjugated secondary antibodies (Bio-Rad) and SuperSignal West Pico Plus (Thermo Fisher) or Immobilon (Millipore) chemiluminescent substrates. Images were acquired and analyzed for densitometric relationships with a LI-COR C-DiGit scanner using Studio Image software. The CETSA was performed preparatory to Western blotting by treating C2C12 cells for 1 h with 10 μM DIPQUO or inactive analog BT344 and then harvesting cells using Accutase cell detachment solution (Sigma A6964). Cells were counted and normalized such that each sample at each temperature contained extract from 1×10^6 cells in 100 μl. Cells were resuspended in ice-cold PBS + HALT cocktail and transferred in 100-μl aliquots into thin-walled PCR tubes. Samples were heated in a temperature gradient using a PCR thermocycler (Eppendorf Mastercycler Pro S) for one 10-min cycle, with gradient values noted in figure legends. Samples were flash-frozen in liquid N_2 and thawed on benchtop three consecutive times and then centrifuged 15 min at max speed at 4°. The protein concentration was obtained by BCA assay (Thermo Fisher) using a SpectraMax 340 PC microplate reader at 562 nm absorbance, and equivalent volumes corresponding to 30 μg in the lowest-temperature sample were loaded onto precast gels for all samples in a given series.

ALP staining and activity assays

C2C12 cells were stained for ALP expression after 3 days treatment with 10 μM DIPQUO or inhibitors, or as otherwise noted in figure legends. Cells were briefly fixed in a mixture of 70% acetone/10% formaldehyde/20% citrate, and staining was achieved using the Leukocyte Alkaline Phosphatase Kit (Sigma 86R-1KT). Images were obtained using an AMG EVOS XL imaging system. ALP activity was quantified using the Colorimetric Alkaline Phosphatase Assay Kit (ABCAM 83369) to detect pNPP substrate according to manufacturer's instructions. Activity was quantified in comparison to a standard curve generated at an absorbance at 405 nm using a Molecular Devices SpectraMax 340PC microplate reader and SoftMax Pro v7.0 software. The protein concentration was obtained by BCA assay in triplicate corresponding to each treatment, and the final activity value was calculated as a ratio of total pNPP digested in pmol per microgram of total protein in each sample.

Quantitative RT-PCR

Total RNA was harvested from hSkMSCs using the Qiagen RNEasy kit, and cDNA was generated from 1 μg RNA using SuperScript VILO kit (Thermo Fisher 11754050). Quantitative PCR was performed as previously reported, using a Roche LightCycler 480, and the $\Delta\Delta C_T$ method, with C_T values compared with DMSO-treated controls and normalized to GAPDH expression. Primer pairs were as follows: GAPDH (F: CCTTCATTGACCTCAACTACATG) (R: TGGGATTTCCATTGATGACAAGC); DLX5 (F: CAACTTTGCCCGAGTCTTCA) (R: GTTGAGAGCTTTGCCATAGGAA); OSX (F: TGCTTGAGGAGGAAGTTCAC) (R: AGGTCACTGCCCACAGAGTA); OPN (F: TTGCAGCCTTCTCAGCCAA) (R: GGAGGCAAAAGCAAATCACTG); GPNMB (F: CTGTGAACACAGCCAATGTG) (R: ATGGGGAGATCTTTGAGGAA).

Data availability

All article data for experimental replicates will be provided upon reasonable request. All remaining data are contained within the article. Intellectual property filing for osteogenic use of DIPQUO has progressed to patent cooperation treaty stage, as of 04/01/2020.

Supporting information—This article contains supporting information.

Acknowledgments—The authors acknowledge Dr Benjamin Stein (WCM) for helpful discussions concerning Western blotting analysis of CETSA gradients.

Author contributions—B. C. conceived the study, carried out experiments, and wrote the manuscript; N. W. carried out experiments; Q. Z. carried out experiments, S. C. conceived the study and provided expert advice, T. E. conceived the study and wrote the manuscript; all authors edited and approved the final manuscript.

Funding and additional information—This work was supported by the Weill Cornell Medicine Daedalus Fund for Innovation (B. C.) and by National Institutes of Health R37 HL56182 (T. E.). The content is solely the responsibility of the authors and does not necessarily represent the official views of the National Institutes of Health.

Conflict of interest—The authors declare that they have no conflicts of interest with the contents of this article.

Abbreviations—The abbreviations used are: AD, Alzheimer's disease; ALP, alkaline phosphatase; AZD, AstraZeneca GSK3-β-specific inhibitor AZD2858; BMP, bone morphogenetic protein; CDK, cyclin-dependent kinase; CETSA, cellular thermal shift assay; CHIR, Wnt signaling activator CHIR99021; CHK, checkpoint kinase; DMSO, dimethyl sulfoxide; ERK, extracellular signal–regulated kinase; GSK3-β, glycogen synthase kinase 3-beta; hSkMSCs, human skeletal muscle satellite cells; LRRK2, leucine-rich repeat kinase-2; MAPK, mitogen-activated protein kinase; pNPP, p-nitrophenylphosphate; S396, serine-396; T_m, melting temperature.

References

1. Roos, P. M. (2014) Osteoporosis in neurodegeneration. *J. Trace Elem. Med. Biol.* **28**, 418–421
2. Cornelius, C., Koverech, G., Crupi, R., Di Paola, R., Koverech, A., Lodato, F., Scuto, M., Salinaro, A. T., Cuzzocrea, S., Calabrese, E. J., and Calabrese, V. (2014) Osteoporosis and alzheimer pathology: Role of cellular

stress response and hormetic redox signaling in aging and bone remodeling. *Front. Pharmacol.* **5**, 120
3. Pan, J. X., Tang, F., Xiong, F., Xiong, L., Zeng, P., Wang, B., Zhao, K., Guo, H., Shun, C., Xia, W. F., Mei, L., and Xiong, W. C. (2018) APP promotes osteoblast survival and bone formation by regulating mitochondrial function and preventing oxidative stress. *Cell Death Dis.* **9**, 1077
4. Bradburn, S., McPhee, J. S., Bagley, L., Sipila, S., Stenroth, L., Narici, M. V., Paasuke, M., Gapeyeva, H., Osborne, G., Sassano, L., Meskers, C. G., Maier, A. B., Hogrel, J. Y., Barnouin, Y., Butler-Browne, G., *et al.* (2016) Association between osteocalcin and cognitive performance in healthy older adults. *Age Ageing* **45**, 844–849
5. Cook, B., Rafiq, R., Lee, H., Banks, K. M., El-Debs, M., Chiaravalli, J., Glickman, J. F., Das, B. C., Chen, S., and Evans, T. (2019) Discovery of a small molecule promoting mouse and human osteoblast differentiation via activation of p38 MAPK-beta. *Cell Chem Biol.* **26**, 926–935. e926
6. Rodriguez-Carballo, E., Gamez, B., and Ventura, F. (2016) p38 MAPK signaling in osteoblast differentiation. *Front. Cell Dev. Biol.* **4**, 40
7. Greenblatt, M. B., Shim, J. H., Zou, W., Sitara, D., Schweitzer, M., Hu, D., Lotinun, S., Sano, Y., Baron, R., Park, J. M., Arthur, S., Xie, M., Schneider, M. D., Zhai, B., Gygi, S., *et al.* (2010) The p38 MAPK pathway is essential for skeletogenesis and bone homeostasis in mice. *J. Clin. Invest.* **120**, 2457–2473
8. Chen, G., Deng, C., and Li, Y. P. (2012) TGF-beta and BMP signaling in osteoblast differentiation and bone formation. *Int. J. Biol. Sci.* **8**, 272–288
9. Wu, M., Chen, G., and Li, Y. P. (2016) TGF-beta and BMP signaling in osteoblast, skeletal development, and bone formation, homeostasis and disease. *Bone Res.* **4**, 16009
10. Thouverey, C., and Caverzasio, J. (2015) Focus on the p38 MAPK signaling pathway in bone development and maintenance. *Bonekey Rep.* **4**, 711
11. Ge, C., Xiao, G., Jiang, D., and Franceschi, R. T. (2007) Critical role of the extracellular signal-regulated kinase-MAPK pathway in osteoblast differentiation and skeletal development. *J. Cell Biol.* **176**, 709–718
12. Yu, K., Xu, J., Liu, Z., Sosic, D., Shao, J., Olson, E. N., Towler, D. A., and Ornitz, D. M. (2003) Conditional inactivation of FGF receptor 2 reveals an essential role for FGF signaling in the regulation of osteoblast function and bone growth. *Development* **130**, 3063–3074
13. Valta, M. P., Hentunen, T., Qu, Q., Valve, E. M., Harjula, A., Seppanen, J. A., Vaananen, H. K., and Harkonen, P. L. (2006) Regulation of osteoblast differentiation: A novel function for fibroblast growth factor 8. *Endocrinology* **147**, 2171–2182
14. Fei, Y., Xiao, L., Doetschman, T., Coffin, D. J., and Hurley, M. M. (2011) Fibroblast growth factor 2 stimulation of osteoblast differentiation and bone formation is mediated by modulation of the Wnt signaling pathway. *J. Biol. Chem.* **286**, 40575–40583
15. Peng, X. D., Xu, P. Z., Chen, M. L., Hahn-Windgassen, A., Skeen, J., Jacobs, J., Sundararajan, D., Chen, W. S., Crawford, S. E., Coleman, K. G., and Hay, N. (2003) Dwarfism, impaired skin development, skeletal muscle atrophy, delayed bone development, and impeded adipogenesis in mice lacking Akt1 and Akt2. *Genes Dev.* **17**, 1352–1365
16. Kawamura, N., Kugimiya, F., Oshima, Y., Ohba, S., Ikeda, T., Saito, T., Shinoda, Y., Kawasaki, Y., Ogata, N., Hoshi, K., Akiyama, T., Chen, W. S., Hay, N., Tobe, K., Kadowaki, T., *et al.* (2007) Akt1 in osteoblasts and osteoclasts controls bone remodeling. *PLoS One* **2**, e1058
17. Houschyar, K. S., Tapking, C., Borrelli, M. R., Popp, D., Duscher, D., Maan, Z. N., Chelliah, M. P., Li, J., Harati, K., Wallner, C., Rein, S., Pforringer, D., Reumuth, G., Grieb, G., Mouraret, S., *et al.* (2018) Wnt pathway in bone repair and regeneration - what do we know so far. *Front. Cell Dev. Biol.* **6**, 170
18. Martinez Molina, D., Jafari, R., Ignatushchenko, M., Seki, T., Larsson, E. A., Dan, C., Sreekumar, L., Cao, Y., and Nordlund, P. (2013) Monitoring drug target engagement in cells and tissues using the cellular thermal shift assay. *Science* **341**, 84–87
19. Martinez Molina, D., and Nordlund, P. (2016) The cellular thermal shift assay: A novel biophysical assay for in situ drug target engagement and mechanistic biomarker studies. *Annu. Rev. Pharmacol. Toxicol.* **56**, 141–161
20. Yamauchi, K., and Kurosaka, A. (2009) Inhibition of glycogen synthase kinase-3 enhances the expression of alkaline phosphatase and insulin-like growth factor-1 in human primary dermal papilla cell culture and maintains mouse hair bulbs in organ culture. *Arch. Dermatol. Res.* **301**, 357–365
21. Ye, S., Tan, L., Yang, R., Fang, B., Qu, S., Schulze, E. N., Song, H., Ying, Q., and Li, P. (2012) Pleiotropy of glycogen synthase kinase-3 inhibition by CHIR99021 promotes self-renewal of embryonic stem cells from refractory mouse strains. *PLoS One* **7**, e35892
22. Marsell, R., Sisask, G., Nilsson, Y., Sundgren-Andersson, A. K., Andersson, U., Larsson, S., Nilsson, O., Ljunggren, O., and Jonsson, K. B. (2012) GSK-3 inhibition by an orally active small molecule increases bone mass in rats. *Bone* **50**, 619–627
23. Wada, M. R., Inagawa-Ogashiwa, M., Shimizu, S., Yasumoto, S., and Hashimoto, N. (2002) Generation of different fates from multipotent muscle stem cells. *Development* **129**, 2987–2995
24. Oishi, T., Uezumi, A., Kanaji, A., Yamamoto, N., Yamaguchi, A., Yamada, H., and Tsuchida, K. (2013) Osteogenic differentiation capacity of human skeletal muscle-derived progenitor cells. *PLoS One* **8**, e56641
25. Nusse, R., and Clevers, H. (2017) Wnt/beta-Catenin signaling, disease, and emerging therapeutic modalities. *Cell* **169**, 985–999
26. Duan, P., and Bonewald, L. F. (2016) The role of the wnt/beta-catenin signaling pathway in formation and maintenance of bone and teeth. *Int. J. Biochem. Cell Biol.* **77**, 23–29
27. Lovestone, S., Reynolds, C. H., Latimer, D., Davis, D. R., Anderton, B. H., Gallo, J. M., Hanger, D., Mulot, S., Marquardt, B., Stabel, S., Woodgett, J. R., and Miller, C. C. J. (1994) Alzheimer's disease-like phosphorylation of the microtubule-associated protein tau by glycogen synthase kinase-3 in transfected mammalian cells. *Curr. Biol.* **4**, 1077–1086
28. Wagner, U., Utton, M., Gallo, J. M., and Miller, C. C. (1996) Cellular phosphorylation of tau by GSK-3 beta influences tau binding to microtubules and microtubule organisation. *J. Cell Sci.* **109**(Pt 6), 1537–1543
29. Hooper, C., Killick, R., and Lovestone, S. (2008) The GSK3 hypothesis of Alzheimer's disease. *J. Neurochem.* **104**, 1433–1439
30. Medina, M., Garrido, J. J., and Wandosell, F. G. (2011) Modulation of GSK-3 as a therapeutic strategy on tau pathologies. *Front. Mol. Neurosci.* **4**, 24
31. Evans, D. B., Rank, K. B., Bhattacharya, K., Thomsen, D. R., Gurney, M. E., and Sharma, S. K. (2000) Tau phosphorylation at serine 396 and serine 404 by human recombinant tau protein kinase II inhibits tau's ability to promote microtubule assembly. *J. Biol. Chem.* **275**, 24977–24983
32. Kimura, T., Ishiguro, K., and Hisanaga, S. (2014) Physiological and pathological phosphorylation of tau by Cdk5. *Front. Mol. Neurosci.* **7**, 65
33. Pei, J. J., An, W. L., Zhou, X. W., Nishimura, T., Norberg, J., Benedikz, E., Gotz, J., and Winblad, B. (2006) P70 S6 kinase mediates tau phosphorylation and synthesis. *FEBS Lett.* **580**, 107–114
34. Jhang, K. A., Park, J. S., Kim, H. S., and Chong, Y. H. (2017) Resveratrol ameliorates tau hyperphosphorylation at Ser396 site and oxidative damage in rat hippocampal slices exposed to vanadate: Implication of ERK1/2 and GSK-3beta signaling cascades. *J. Agric. Food Chem.* **65**, 9626–9634
35. Stepanov, A., Karelina, T., Markevich, N., Demin, O., and Nicholas, T. (2018) A mathematical model of multisite phosphorylation of tau protein. *PLoS One* **13**, e0192519
36. Planel, E., Tatebayashi, Y., Miyasaka, T., Liu, L., Wang, L., Herman, M., Yu, W. H., Luchsinger, J. A., Wadzinski, B., Duff, K. E., and Takashima, A. (2007) Insulin dysfunction induces *in vivo* tau hyperphosphorylation through distinct mechanisms. *J. Neurosci.* **27**, 13635–13648
37. Li, J., Deng, J., Sheng, W., and Zuo, Z. (2012) Metformin attenuates Alzheimer's disease-like neuropathology in obese, leptin-resistant mice. *Pharmacol. Biochem. Behav.* **101**, 564–574
38. Kimura, T., Sharma, G., Ishiguro, K., and Hisanaga, S. I. (2018) Phospho-tau bar code: Analysis of phosphoisotypes of tau and its application to tauopathy. *Front. Neurosci.* **12**, 44
39. Gillespie, J. R., Bush, J. R., Bell, G. I., Aubrey, L. A., Dupuis, H., Ferron, M., Kream, B., DiMattia, G., Patel, S., Woodgett, J. R., Karsenty, G., Hess, D. A., and Beier, F. (2013) GSK-3beta function in bone regulates skeletal development, whole-body metabolism, and male life span. *Endocrinology* **154**, 3702–3718

40. Zamani, A., Omrani, G. R., and Nasab, M. M. (2009) Lithium's effect on bone mineral density. *Bone* **44**, 331–334
41. Li, L., Peng, X., Qin, Y., Wang, R., Tang, J., Cui, X., Wang, T., Liu, W., Pan, H., and Li, B. (2017) Acceleration of bone regeneration by activating Wnt/beta-catenin signalling pathway via lithium released from lithium chloride/calcium phosphate cement in osteoporosis. *Sci. Rep.* **7**, 45204
42. Sisask, G., Marsell, R., Sundgren-Andersson, A., Larsson, S., Nilsson, O., Ljunggren, O., and Jonsson, K. B. (2013) Rats treated with AZD2858, a GSK3 inhibitor, heal fractures rapidly without endochondral bone formation. *Bone* **54**, 126–132
43. Bhat, R. V., Andersson, U., Andersson, S., Knerr, L., Bauer, U., and Sundgren-Andersson, A. K. (2018) The conundrum of GSK3 inhibitors: Is it the dawn of a new beginning? *J. Alzheimers Dis.* **64**, S547–S554
44. Freland, L., and Beaulieu, J. M. (2012) Inhibition of GSK3 by lithium, from single molecules to signaling networks. *Front. Mol. Neurosci.* **5**, 14
45. Beurel, E., Grieco, S. F., and Jope, R. S. (2015) Glycogen synthase kinase-3 (GSK3): Regulation, actions, and diseases. *Pharmacol. Ther.* **148**, 114–131